In Situ Transmission Electron Microscopy Observation of the Conversion Mechanism of Fe_2O_3/Graphene Anode during Lithiation–Delithiation Processes

Qingmei Su,[†,‡] Dong Xie,[†] Jun Zhang,[†] Gaohui Du,[†,*] and Bingshe Xu[‡]

[†]Institute of Physical Chemistry, Zhejiang Normal University, Jinhua 321004, China and [‡]College of Materials Science and Engineering, Taiyuan University of Technology, Taiyuan 030024, Shanxi, China

ABSTRACT Transition metal oxides have attracted tremendous attention as anode materials for lithium ion batteries (LIBs) recently. However, their electrochemical processes and fundamental mechanisms remain unclear. Here we report the direct observation of the dynamic behaviors and the conversion mechanism of Fe_2O_3/graphene in LIBs by *in situ* transmission electron microscopy (TEM). Upon lithiation, the Fe_2O_3 nanoparticles showed obvious volume expansion and morphological changes, and the surfaces of the electrode were covered by a nanocrystalline Li_2O layer. Single-crystalline Fe_2O_3 nanoparticles were found to transform to multicrystalline nanoparticles consisting of many Fe nanograins embedded in Li_2O matrix. Surprisingly, the delithiated product was not Fe_2O_3 but FeO, accounting for the irreversible electrochemical process and the large capacity fading of the anode material in the first cycle. The charge–discharge processes of Fe_2O_3 in LIBs are different from previously recognized mechanism, and are found to be a fully reversible electrochemical phase conversion between Fe and FeO nanograins accompanying the formation and disappearance of the Li_2O layer. The macroscopic electrochemical performance of Fe_2O_3/graphene was further correlated with the microcosmic *in situ* TEM results.

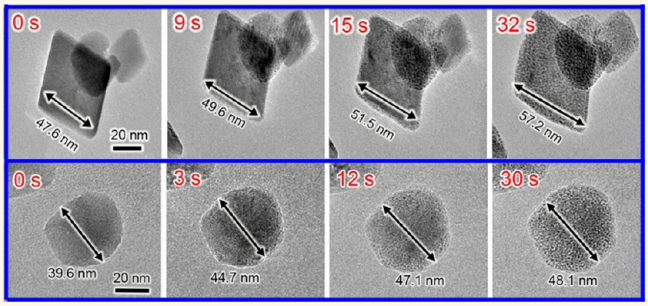

KEYWORDS: metal oxide · transmission electron microscopy · lithium ion battery · conversion mechanism

Iron oxides (Fe_2O_3) have attracted much attention as one of the most promising candidates as anode materials for lithium ion batteries (LIBs) owing to large capacities, low cost, ease of fabrication and low toxicity.[1−3] The electrochemical process of Fe_2O_3 in LIBs is the conversion mechanism involving the reduction and oxidation reaction between iron oxide and lithium. A large specific volume change commonly occurs in the host matrix of iron oxides during the electrochemical conversion processes, resulting in pulverization of the electrodes and subsequent loss of electrical contacts between the active material and current collector.[4,5] To circumvent these obstacles, previous reports show that a stable cycling can be achieved by fabricating nanostructured iron oxides,[6] or incorporating iron oxide nanoparticles with carbon materials.[7] In well-designed electrodes, carbon materials not only act as a buffer to accommodate the strain associated with the volume change during the lithium insertion/extraction processes, but also improve the lithium diffusion in electrodes and increase the electric conductivity, leading to significantly improved electrochemical performance.[8−11]

Although the electrochemical performances of Fe_2O_3 have been greatly enhanced by various techniques, a few of the fundamental questions concerning the reaction process remain unclear. Nano-sized transition-metal oxides as anode materials for LIBs were first reported by Tarascon *et al.*;[12] they demonstrated that the electrochemical process of CoO is $CoO + 2Li \leftrightarrow Li_2O + Co$ by *ex situ* TEM. Subsequently,

* Address correspondence to gaohuidu@zjnu.edu.cn.

Received for review July 19, 2013 and accepted September 9, 2013.

Published online September 09, 2013
10.1021/nn403720p

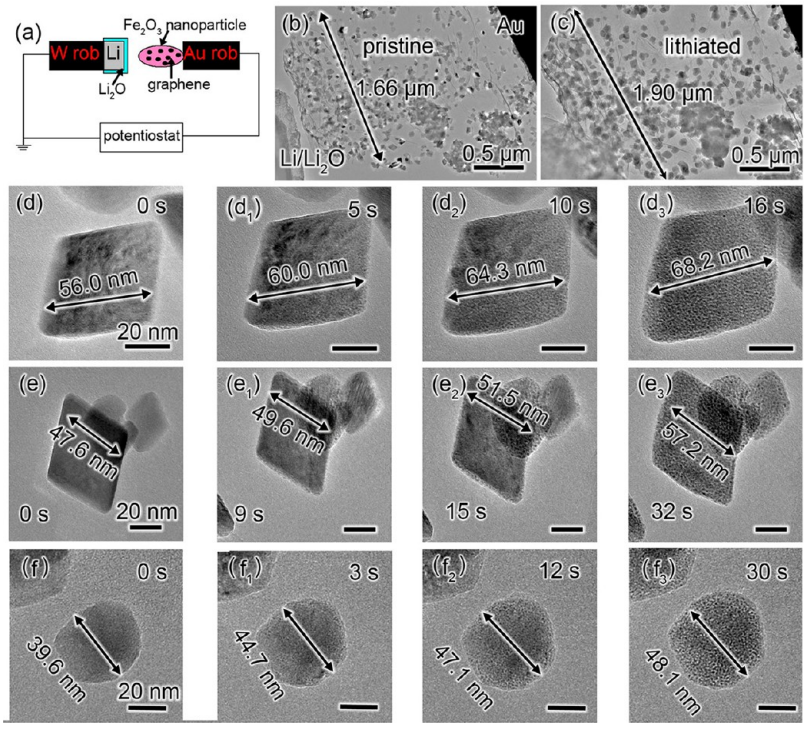

Figure 1. (a) Schematic illustration of the *in situ* experimental setup. (b) The corresponding TEM image of the nano-LIB constructed inside the TEM. (c) Fe_2O_3/graphene electrode after lithiation with a potential of −1 V. (d−f) Electrochemical lithiation of individual Fe_2O_3 nanoparticles anchored on graphene nanosheet showing obvious volume expansion as a function of time. The scale bars are 20 nm.

other transition-metal oxides as anode materials for LIBs have been extensively studied and their electrochemical processes have been proposed according to the conversion mechanisms.[13−15] As for Fe_2O_3, its electrochemical reaction in LIBs was referred to as $Fe_2O_3 + 6Li \leftrightarrow 2Fe + 3Li_2O$ with the absence of experimental evidence in many literatures.[2,3] It is well-known that there exists a large capacity fading in the first charge−discharge cycle, which is generally attributed to the irreversible electrochemical process such as the solid electrolyte interphase (SEI) layer formation and electrode pulverization. In fact, the nature of irreversible electrochemical process and its influence on the conversion mechanism are still not fully understood. In particular, the microscopic conversation process of transition metal oxide in LIBs is in a black box.

In situ TEM studies on the lithiation−delithiation of electrode materials in LIBs have been reported recently, permitting an electrochemical reaction to be observed inside a TEM.[16−21] In this paper, we constructed an all-solid nano-LIB using an individual Fe_2O_3/graphene as anode inside a high-resolution TEM; the Fe_2O_3 nanoparticles were well dispersed on an individual graphene sheet to enable direct real-time visualization of the electrochemical processes. The evolution of Fe_2O_3 nanoparticles was monitored by simultaneous determination of the microstructure with high-resolution TEM, electron diffraction (ED), and electron energy-loss spectroscopy (EELS). A deep understanding on the electrochemical behavior and conversion mechanism of Fe_2O_3 has been achieved.

RESULTS AND DISCUSSION

The nanoscale electrochemical LIB device to enable direct observation is schematically illustrated in Figure 1a. The Fe_2O_3/graphene composite was attached to a gold wire and used as the working electrode. A Li metal attached to a tungsten wire was served as the counter electrode and lithium source, and the naturally grown Li_2O layer on the surface of Li metal was used as a solid-state electrolyte to allow the transport of Li^+ ions. Both the Fe_2O_3/graphene and lithium electrodes were mounted onto a Nanofactory STM-TEM holder to realize the electrochemical reaction in TEM. Figure 1b is a TEM image of the nano-LIB constructed inside the TEM. The initial width of the graphene sheet was 1.66 μm. A typical lithiation experiment was conducted by applying a constant potential of −1 V to the Fe_2O_3/graphene with respect to the Li counter electrode to drive the electrons and Li^+ ions flow across the circuit after the two electrodes were contacted (Figure 1c). It was found that the width of the graphene sheet increased to 1.90 μm after lithiation. Actually, the observed lateral size change was not a real lattice expansion but resulted from the tilting and expanding from corrugated graphene to a flat one due to the large stress caused by the lithium intercalation into the

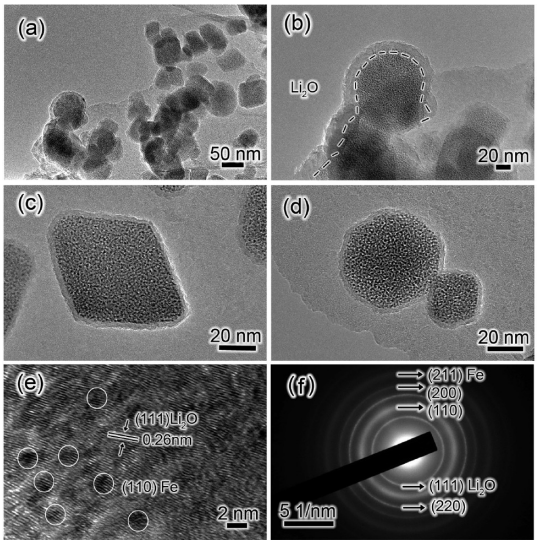

Figure 2. (a and b) TEM images of Fe_2O_3/graphene electrode after the first lithiation. (c and d) TEM images of lithiated nanoparticles showing the formation of Li_2O layer. (e) HRTEM image of a lithiated nanoparticle. The white circles denote the Fe nanograins. (f) ED pattern of the lithiated electrode.

(0002) planes.[19] Movies have been captured to reveal the dynamic reaction process of individual Fe_2O_3 nanoparticles (see Supporting Information for the movies). Figure 1d−f shows a time sequence of TEM video images of a few nanoparticles in the lithiation process. A rhombic Fe_2O_3 nanoparticle in Figure 1d was fully lithiated within 16 s, and its size expanded from 56 nm to about 68.2 nm after lithiation (Figure 1d_3). As the lithium diffused on graphene, the lithiation of three neighboring nanoparticles occurred (Figure 1e). Similarly, the rhombic particle showed a size expansion from 47.6 to 57.2 nm in the lithiation process. The morphological expansion during the lithiation exhibits slightly anisotropic, as can be revealed by the lithiated nanoparticles in Figure 1d_3,e_3). Figure 1f show the lithiation process of a spherical Fe_2O_3 nanoparticle, which displays a size expansion from 39.6 to 48.1 nm within 30 s. The lithiation ratio of these three Fe_2O_3 nanoparticles is about 1.75, 0.74, and 0.66 nm/s, respectively, which should be dependent on the local Li^+ concentration around the particles. The volume expansion of the three particles is estimated to be 80.6%, 73.5%, and 79.7%, respectively, based on their size increases. We further checked eight spherical nanoparticles, and their volume expansions range from 70% to 83.3% with a mean value of 74.7%. Besides the obvious morphology and volume changes, the microstructure of each Fe_2O_3 nanoparticle has evolved from a single crystal to a particle with numerous Fe nanograins embedded in the Li_2O matrix during the lithiation process. Interestingly, all the Fe_2O_3 nanoparticles have no cracking or fracture in the lithiation process, which is different from the lithiation of Si particles.[20]

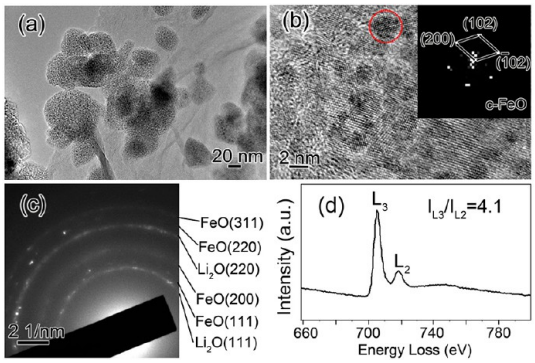

Figure 3. (a) TEM image of a Fe_2O_3/graphene electrode after the first delithiation process. (b) HRTEM image of a delithiated nanoparticle. Inset of (b) is the FFT pattern of the nanograin marked by red circle. (c) ED pattern and (d) EELS spectrum of the delithiated electrode.

Figure 2a,b is the TEM images of a Fe_2O_3/graphene electrode after the first lithiation. We can clearly see that the surfaces and edges of the Fe_2O_3/graphene were coated by a uniform layer of crystallites with a thickness around 3−10 nm, which was identified to be Li_2O from the ED pattern in Figure 2f. The TEM images of individual Fe_2O_3 nanoparticles with different shapes after the first lithiation are displayed in Figure 2c,d. Obviously, the Li_2O shells with a uniform thickness of ~5 nm were formed on the surface of the lithiated nanoparticles irrespective of their shapes. Figure 2e,f shows the detailed structure information on the lithiated electrode. In the HRTEM image of a lithiated Fe_2O_3 nanoparticle in Figure 2e, the lattice spacing is measured to be 0.26 nm, which is consistent with the lattice spacing of (111) plane of Li_2O (JCPDS no. 77-2144). The lattice fringes of the circled nanograins are in agreement with the (110) plane of body-centered cubic (bcc) Fe (JCPDS no. 87-0722). The ED pattern of the lithiated Fe_2O_3 also demonstrates the lithiation reaction involves the formation of Li_2O accompanying the reduction of Fe_2O_3 nanoparticles to bcc Fe nanograins (Figure 2f). Therefore, the first lithiation of Fe_2O_3 nanoparticles as anode can be expressed as the electrochemical process: $Fe_2O_3 + 6Li^+ + 6e^- \rightarrow 2Fe + 3Li_2O$.

After the first full lithiation process, a potential of +2.5 V was applied to the lithiated electrode with respect to the Li counter electrode to initiate the delithiation, and the results are shown in Figure 3. Figure 3a is a representative TEM image of the delithiated electrode. It can be clearly seen that the thin Li_2O layers almost disappeared. However, a thin layer of Li_2O still remained on the surface of the graphene after delithiation due to irreversible reaction. The HRTEM image of a delithiated nanoparticle is shown in Figure 3b. The corresponding fast Fourier transform (FFT) pattern of the marked nanograin in the HRTEM image is given in the inset, which can be indexed as the cubic FeO (JCPDS no. 89-2468) and indicates the possible formation of FeO nanograins in the

delithiated process. This conjecture is confirmed by the ED pattern of the delithiated Fe_2O_3/graphene electrode as shown in Figure 3c; the diffraction rings can be perfectly indexed as a mixture of face-centered cubic (fcc) FeO and fcc Li_2O (JCPDS no. 77-2144). It is surprising that no Fe_2O_3 phase is detected after the delithiation. EELS spectrum is widely used to investigate the valence states since the $L_{2,3}$ edges from the 3d transition elements exhibit structures that are sensitive to the valence state of the metals. Here, the EELS spectrum of a delithiated nanoparticle is shown in Figure 3(d). The L_3/L_2 intensity ratio of Fe elements at delithiated state is 4.1, corresponding to the valence state of 2+,[22,23] in good agreement with the HRTEM and ED results. Based on the analysis, we conclude that the delithiation process can not convert the oxide electrode to its original state, namely Fe_2O_3. It indicates that the Fe_2O_3 anode undergoes irreversible structural changes during the first lithiation/delithiation process. Noticeably, Li_2O was still detected in the delithiated electrode, which suggested the existence of a certain number of Li^+ ions in the form of Li_2O after delithiation. Li_2O has been reported to be electrochemically inactive, which was confirmed by failed attempts to electrochemically decompose Li_2O powders even when mechanically milled with Co powders in previous work.[12] The electrochemically driven size confinement of the metal particles was thus believed to enhance their electrochemical activity toward the formation/decomposition of Li_2O.[12] As for Fe_2O_3 electrode in our experiments, the decomposition of Li_2O can be attributed to the electrocatalysis of Fe nanograins within the Li_2O matrix. FeO nanograins form when the delithiation reaction proceeds. We propose that the electrocatalytic activity of FeO is much weaker as compared to Fe nanograins so that the electrochemical reaction ceases after full conversion from Fe to FeO in the electrode. So the inactive Li_2O remains as a result of the irreversible electrochemical conversion.

To understand the electrochemical charge−discharge process of Fe_2O_3/graphene anode during cycling, *in situ* TEM experiments were conducted to reveal the continual lithiation−delithiation induced microstructure evolution in an individual Fe_2O_3/graphene electrode. In the experiments, the potentials of −1 and +3 V were alternately applied to the Fe_2O_3/graphene anode against the Li counter electrode to initiate the lithiation and delithiation reaction. The morphology and phase changes during the first two charge−discharge cycles are displayed in Figure 4. Figure 4a is a TEM image of the pristine Fe_2O_3/graphene and shows the Fe_2O_3 nanoparticles with sizes around 20−50 nm were anchored on graphene. The ED pattern of the pristine electrode is shown in Figure $4a_1$. It can be indexed as the rhomb-centered crystal structure of Fe_2O_3 (JCPDS no. 89-2810). After the first lithiation process (Figure 4b), the pristine Fe_2O_3

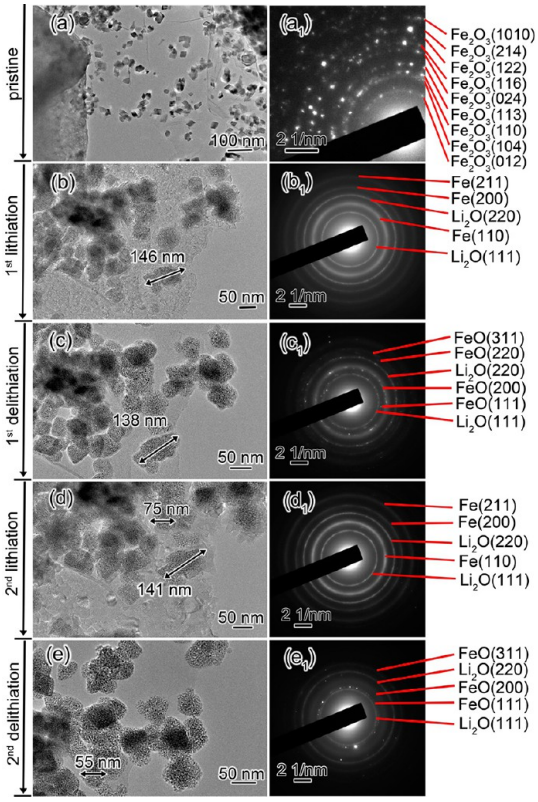

Figure 4. Morphology and structure evolution of Fe_2O_3/graphene electrode upon cycling with the potential of −1 V for lithiation and +3 V for delithiation. (a) The pristine Fe_2O_3/graphene electrode. The electrode after the first lithiation (b), the first delithiation (c), the second lithiation (c), and the second delithiation (d). (a_1−e_1) are the corresponding ED patterns of the electrode in (a−e).

nanoparticles were inflated and expanded in size, and a thin layer of Li_2O crystallites was formed on the Fe_2O_3 nanoparticles and graphene sheet. A typically lithiated Fe_2O_3 nanoparticle with a size of 146 nm was anchored on the graphene. The corresponding ED pattern of the lithiated electrode is shown in Figure $4b_1$; the diffraction rings can be well indexed to bcc Fe and fcc Li_2O, suggesting the conversion of Fe_2O_3 to Fe in the first lithiation process. The delithiation process was initiated by applying a +3 V potential to the Fe_2O_3/graphene electrode. The marked nanoparticles shrank from 146 to 138 nm in size, and the Li_2O layer gradually shrank and almost disappeared after full delithiation (Figure 4c). Figure $4c_1$ displays the ED pattern of the delithiated electrode, which can be well indexed to cubic FeO and cubic Li_2O. The ED pattern revealed the remains of Li_2O after delithiation, which can account for the irreversibility in the first cycle. The second lithiation process proceeded with the −1 V potential again (Figure 4d). The marked particle expanded to about 141 nm, and the Li_2O layer thickened and continued to cover the electrode like the first lithiation. The ED pattern of the second lithiated electrode is shown in Figure $4d_1$ and can be indexed as bcc Fe and cubic Li_2O. The Li_2O layer thinned again in the second

delithiation process (Figure 4e), showing the reversible change. The denoted nanoparticle shrank from 75 to 55 nm, and the ED pattern showed the resultant Fe nanograins transformed to FeO nanograins again in the second delithiation process. We also examined the phase transformation of a single Fe_2O_3 nanoparticle during the lithiation and delithiation cycles as shown in Figure S1 in Supporting Information, which reveals the same conversion as we discussed above. A noticeable phenomenon is that a few extremely strong spots can be observed in the Fe (110) diffraction ring (Figure S1(b1)); the nonuniform intensity suggests the presence of preferentially orientated Fe nanograins in the first lithiated particle. The feature of orientated array still persists for the subsequently formed FeO nanograins in the first delithiated particle, and it becomes weak since the second cycle. All the TEM results imply the reversible conversion from Fe to FeO rather than Fe_2O_3 after the first lithiation process. This can account for the large capacity fading during the first cycle due to the lower theoretical capacity of FeO as compared to Fe_2O_3. These cycles indicate that the reversible electrochemical conversion between Fe and FeO takes place after the first cycle, and the electrochemical reaction can be expressed as $Fe + Li_2O \leftrightarrow FeO + 2Li^+ + 2e^-$.

EELS technique is ideally suited for studying core-loss edges below energy loss of 2 keV. The $L_{2,3}$ "white lines" which arise from dipole transitions to unoccupied d states show valence-specific structures and can be used as valence fingerprints. Here, the white-line intensity ratio (L_3/L_2) has been analyzed to correlate EELS features with the oxidation states of Fe in the lithiated and delithiated products. EELS experiments were performed in the electrochemical process during the first two cycles to reveal the change of chemical valence of Fe elements (as shown in Figure 5). Figure 5a displays the EELS spectrum of Fe in the electrode at the initial state, and the L_3/L_2 intensity ratio was 5.1, corresponding to the valence state of 3+.[22] After the first lithiation reaction, the L_3/L_2 intensity ratio reduced to 2.8 in Figure 5b, which indicated the oxide state transition of Fe from 3+ to zero.[23] Figure 5c show the Fe $L_{2,3}$ edge peaks of the electrode after the first delithiation process, and the L_3/L_2 intensity ratio increased to 4.3, corresponding to the valence state of 2+. It confirmed that the delithiated product was not Fe_2O_3 but FeO. In the second cycle of lithiation/delithiation process, the similar reversal of L_3/L_2 intensity ratio was also observed. The repeated changes in the intensity ratio suggest that Fe underwent a reversible transition between Fe^0 and Fe^{2+} in the electrochemical process. Combining with the ED results shown in Figure 4a_1–e_1, we conclude that the reversible electrochemical reaction of the electrode in the lithiation–delithiation process is a phase transition between bcc Fe nanograins and fcc FeO nanograins.

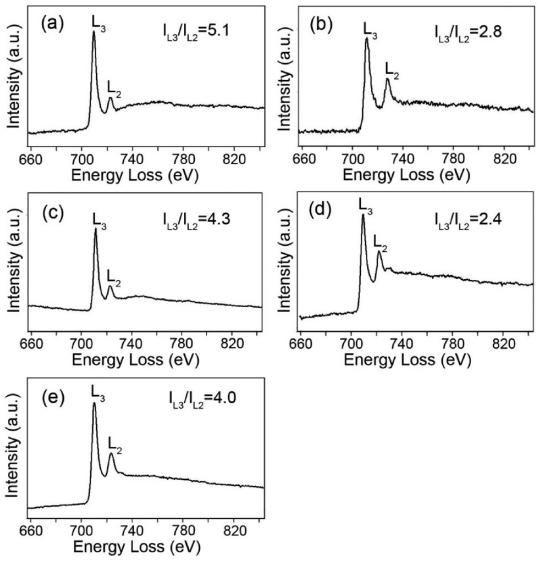

Figure 5. EELS spectra of Fe-$L_{2,3}$ edges of the electrode during the lithiation and delithiation cycles. (a) The initial stage, (b) after the first lithiation and (c) delithiation process, and (d) after the second lithiation and (e) delithiation process.

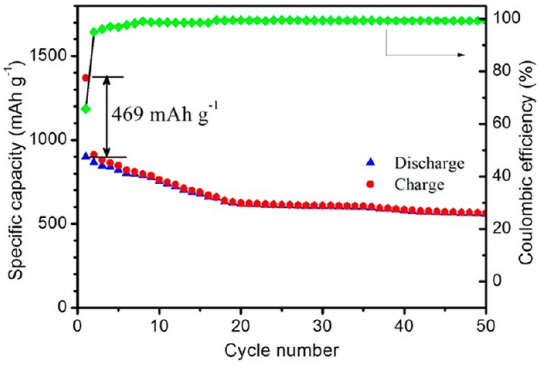

Figure 6. Cycling performance of Fe_2O_3/graphene as anode in LIBs at a current density of 50 mA g^{-1}.

Therefore, the electrochemical cycling of Fe_2O_3 electrode in LIBs can be expressed as:

$$Fe_2O_3 + 6Li^+ + 6e^- \rightarrow 2Fe + 3Li_2O \text{ (first lithiation)}$$

$$Fe + Li_2O \leftrightarrow FeO + 2Li^+ + 2e^-$$
$$\text{(subsequent delithiation/lithiation)}$$

According to the above electrochemical process, there is a large discharge/charge capacity fading in the first cycle due to the lower theoretical capacity of FeO (744 mAh g^{-1}) than that of Fe_2O_3 (1005 mAh g^{-1}). We can obtain that the theoretical capacity loss is about 335 mAh g^{-1} due to the irreversible phase conversion. Galvanostatic cycling was performed on coin-type half cells to correlate the macroscopic electrochemical properties of Fe_2O_3/graphene with the microcosmic *in situ* TEM results. As shown in Figure 6, the Fe_2O_3/graphene electrode delivers an initial discharge capacity of 1369 mAh g^{-1} and a charge capacity of 899 mAh g^{-1} with a Coulombic efficiency of

65.7% in the first cycle. The discharge/charge capacities are almost the same in each cycle with a Coulombic efficiency of >95% during the subsequent cycles, indicating an excellent cycling performance after the first cycle. The initial capacity fading of Fe_2O_3/graphene electrode is 469 mAh g^{-1}. To exclude the effect of graphene, we also checked other reports on the capacity fading of pure Fe_2O_3 as anode in the first cycle, and it is found to be 398 mAh g^{-1} for porous Fe_2O_3 microspheres,[24] 420 mAh g^{-1} for Fe_2O_3 mesoporous nanoparticles[25] and hollow microcubes,[26] and 405 mAh g^{-1} for hollow a-Fe_2O_3 spheres.[27] The average initial capacity loss for pure Fe_2O_3 is 411 mAh g^{-1}. The initial capacity loss of the electrodes in LIBs is generally attributed to the electrode pulverization, the irreversible electrochemical decomposition of electrolyte and the subsequent formation of a SEI layer on the surface.[28] Our result reveals that the nature of the initial capacity fading of Fe_2O_3 is the irreversible phase conversion, which is responsible for around 82% of the total capacity loss; about 18% of the capacity loss can be caused by other irreversible electrochemical processes.

CONCLUSION

We have studied the electrochemical lithiation–delithiation process of Fe_2O_3 using *in situ* TEM. Direct observation on the structure and phase evolution of the electrode during electrochemical cycles has been achieved. The results reveal that single-crystalline Fe_2O_3 nanoparticles transform to multicrystalline nanoparticles consisting of many BCC Fe nanograins embedded in Li_2O matrix during the first lithiation. Typically, a uniform layer of Li_2O can be observed on the lithiated electrode, which almost disappears after delithiation. The remains of Li_2O after delithiation indicate the irreversible electrochemical reaction in the charge–discharge process. Moreover, the delithiated product is found to be FeO instead of Fe_2O_3. The irreversible phase conversion could be caused by the weak electrocatalytic activity of FeO as compared to Fe nanograins. The electrochemical charge–discharge processes of Fe_2O_3 nanoparticles as anode in LIBs are revealed to be reversible phase transitions between bcc Fe nanograins and fcc FeO nanograins. The irreversible changes of the Fe_2O_3 electrode in the first charge–discharge process consist of the irreversible phase conversion and other irreversible electrochemical process, while the former is responsible for about 82% of the initial capacity loss. The electrochemical mechanism could also be applied to other metal oxide, *e.g.*, Co_3O_4 and Mn_3O_4. Our study provides direct evidence and profound insight into the reaction mechanism governing the metal oxide anode performance in LIBs.

EXPERIMENTAL SECTION

Preparation of Fe_2O_3/Graphene. Graphite oxide was prepared by a modified Hummer's method.[29] To synthesize the Fe_2O_3/graphene, graphene oxide (69 mg), $FeCl_3 \cdot 6H_2O$ (2 mmol), and CH_3COONa (6 mmol) were added to 40 mL of deionized water. After sonication for several hours, the solution was transferred to a Teflon-lined stainless steel autoclave (50 mL) and heated in an oven at 160 °C for 18 h, and then cooled to room temperature naturally. The obtained product was subsequently separated by centrifugation, washed with distilled water and ethanol, and dried at 60 °C for 12 h. TEM analysis revealed that the as-prepared graphene sheets have 3–6 layers with a thickness of 1–2 nm.

***In Situ* Electrochemical Experiments.** The *in situ* nanoscale electrochemical experiments were carried out using a Nanofactory TEM-scanning tunneling microscopy (STM) holder in a JEOL JEM-2100F TEM. Briefly, the electrochemical setup consisted of an individual Fe_2O_3/graphene nanosheet as the working electrode, a layer of Li_2O solid electrolyte, and a bulk Li metal as the counter electrode. The detailed procedures are as follows: a 0.25 mm-thick gold rod was cut to produce a clean and fresh cross section; then Fe_2O_3/graphene was glued to the pretreated gold rod with conductive epoxy as the working electrode. A sharp tungsten STM tip was used to scratch Li metal surface to fetch some fresh Li inside a glovebox filled with argon. The layer of Li on the tip of the W rod was served as the counter electrode and lithium source. Both the Fe_2O_3/graphene and lithium electrodes were mounted onto a Nanofactory STM-TEM holder inside the same glovebox. The holder was quickly transferred into the TEM column; a native Li_2O layer formed on the surface of Li metal due to the exposure to air, which was served as the solid-state electrolyte to allow the transport of Li^+ ions. The Li_2O/Li electrode was mounted on the mobile STM probe, which could be driven to contact the Fe_2O_3/graphene electrode inside the TEM. Lithiation took place after a negative bias was applied on the Fe_2O_3/graphene with respect to the lithium metal to drive Li^+ transport through the solid-state Li_2O layer, and the bias was then reversed to positive to facilitate delithiation.

Half Cell Measurement. The electrochemical cycling experiments were performed at a CT2001A Land battery tester at room temperature. To prepare the LIB anode, the electrode slurry was made by mixing the active material, acetylene black, and polyvinylidene fluoride (PVDF) in a weight ratio of 75:15:10 in *N*-methyl pyrrolidone with stirring for 2 h. The working electrodes were made by spreading the slurry onto a Ni foam current collector and drying at 120 °C under vacuum overnight. The electrolyte solution was 1 M $LiPF_6$ dissolved in ethylene carbonate (EC)/dimethyl carbonate (DMC) (1:1, v/v). Pure Li foil (Aldrich) was used as the counter electrode. The cells were charged and discharged between 0.01 and 3 V (*vs* Li/Li^+) at a current density of 50 mA g^{-1}.

Conflict of Interest: The authors declare no competing financial interest.

Acknowledgment. This work was supported by the Program for New Century Excellent Talents in University of Ministry of Education of China (NCET-11-1081) and the National Science Foundation of China (No. 21203168).

Supporting Information Available: Three movies (avi) showing the lithiation process of individual Fe_2O_3 nanoparticles; the TEM images and ED patterns of an individual nanoparticle during the lithiation–delithiation cycles. This material is available free of charge *via* the Internet at http://pubs.acs.org.

REFERENCES AND NOTES

1. Koo, B.; Xiong, H.; Slater, M. D.; Prakapenka, V. B.; Balasubramanian, M.; Podsiadlo, P.; Johnson, C. S.; Rajh, T.;

Shevchenko, E. V. Hollow Iron Oxide Nanoparticles for Application in Lithium Ion Batteries. *Nano Lett.* **2012**, *12*, 2429–2435.
2. Zhang, L.; Wu, H. B.; Madhavi, S.; Hng, H. H.; Lou, X. W. Formation of Fe_2O_3 Microboxes with Hierarchical Shell Structures from Metal-Organic Frameworks and their Lithium Storage Properties. *J. Am. Chem. Soc.* **2012**, *134*, 17388–17391.
3. Xu, J. S.; Zhu, Y. J. Monodisperse Fe_3O_4 and γ-Fe_2O_3 Magnetic Mesoporous Microspheres as Anode Materials for Lithium-Ion Batteries. *ACS Appl. Mater. Interfaces* **2012**, *4*, 4752–4757.
4. Zhu, X. J.; Zhu, Y. W.; Murali, S.; Stollers, M. D.; Ruoff, R. S. Nanostructured Reduced Graphene Oxide/Fe_2O_3 Composite as a High-Performance Anode Material for Lithium Ion Batteries. *ACS Nano* **2011**, *5*, 3333–3338.
5. Ban, C. M.; Wu, Z. C.; Gillaspie, D. T.; Chen, L.; Yan, Y. F.; Blackburn, J. L.; Dillon, A. C. Nanostructured Fe_3O_4/SWNT Electrode: Binder-Free and High-Rate Li-Ion Anode. *Adv. Mater.* **2010**, *22*, E145–E149.
6. Chen, J. S.; Zhu, T.; Yang, X. H.; Yang, H. G.; Lou, X. W. Top-Down Fabrication of *a*-Fe_2O_3 Single-Crystal Nanodiscs and Microparticles with Tunable Porosity for Largerly Improved Lithium Storage Properties. *J. Am. Chem. Soc.* **2010**, *132*, 13162–13164.
7. Jang, B.; Park, M.; Chae, O. B.; Park, S.; Kim, Y.; Oh, S. M.; Piao, Y. Z.; Hyeon, T. Direct Synthesis of Self-Assembled Ferrite/Carbon Hybrid Nanosheets for High Performance Lithium-Ion Battery Anode. *J. Am. Chem. Soc.* **2012**, *134*, 15010–15015.
8. Liu, S. Y.; Xie, J.; Pan, Q.; Wu, C. Y.; Cao, G. S.; Zhu, T. J.; Zhao, X. B. Graphene Anchored with Nanocrystal Fe_2O_3 with Improved Electrochemical Li-Storage Properties. *Int. J. Electrochem. Sci.* **2012**, *7*, 354–362.
9. Yang, S. B.; Sun, Y.; Chen, L.; Hernandez, Y.; Feng, X. L.; Müllen, K. Porous Iron Oxide Ribbons Grown on Graphene for High-Performance Lithium Storage. *Sci. Rep.* **2012**, *2*, 427.
10. Wu, Z. S.; Ren, W. C.; Xu, L.; Li, F.; Cheng, H. M. Doped Graphene Sheets as Anode Materials with Super High Rate and Large Capacity for Lithium Ion Batteries. *ACS Nano* **2011**, *5*, 5463–5471.
11. Latorre-Sanchez, M.; Atienzar, P.; Abellán, G.; Puche, M.; Fornés, V.; Ribera, A.; García, H. The Synthesis of a Hybrid Graphene-Nickel/Manganese Mixed Oxide and Its Performance in Lithium-Ion Batteries. *Carbon* **2012**, *50*, 518–525.
12. Poizot, P.; Laruelle, S.; Grugeon, S.; Dupont, L.; Tarascon, J. M. Nano-Sized Transition-Metal Oxides as Nagative Electrode. *Nature* **2000**, *407*, 496–499.
13. Ko, S.; Lee, J. I.; Yang, H. S.; Park, S.; Jeong, U. Mesoporous CuO Particles Threated with CNTs for High-Performance Lithium-Ion Battery Anodes. *Adv. Mater.* **2012**, *24*, 4451–4456.
14. Peng, C. X.; Chen, B. D.; Qin, Y. Facile Ultrasonic Synthesis of CoO Quantum Dot/Graphene Nanosheet Composites with High Lithium Storage Capacity. *ACS Nano* **2012**, *6*, 1074–1081.
15. Xie, D.; Yuan, W. W.; Dong, Z. M.; Su, Q. M.; Zhang, J.; Du, G. H. Facile Synthesis of Porous NiO Hollow Microspheres and Its Electrochemical Lithium-Storage Performance. *Electrochim. Acta* **2013**, *92*, 87–92.
16. Huang, J. Y.; Zhong, L.; Wang, C. M.; Sullivan, J. P.; Xu, W.; Zhang, L. Q.; Mao, S. X.; Hudak, N. S.; Liu, X. H.; Subramanian, A.; *et al. In Situ* Observation of the Electrochemical Lithiation of a Single SnO_2 Nanowire Electrode. *Science* **2010**, *330*, 1515–1520.
17. Liu, X. H.; Zheng, H.; Zhong, L.; Huang, S.; Karki, K.; Zhang, L. Q.; Liu, Y.; Kushima, A.; Liang, W. T.; Wang, J. W.; *et al.* Anisotropic Swelling and Fracture of Silicon Nanowires during Lithiation. *Nano Lett.* **2011**, *11*, 3312–3318.
18. Liu, X. H.; Huang, S.; Picraux, S. T.; Li, J.; Zhu, T.; Huang, J. Y. Reversible Nanopore Formation in Ge Nanowires during Lithiation-Delithiation Cycling: An *In Situ* Transmission Electron Microscopy Study. *Nano Lett.* **2011**, *11*, 3991–3997.
19. Su, Q. M.; Chang, L.; Zhang, J.; Du, G. H.; Xu, B. S. *In Situ* TEM Observation of the Electrochemical Process of Individual CeO_2/Graphene Anode for Lithium Ion Battery. *J. Phys. Chem. C* **2013**, *117*, 4292–4298.
20. Liu, X. H.; Zhong, L.; Huang, S.; Mao, S. X.; Zhu, T.; Huang, J. Y. Size-Dependent Fracture of Silicon Nanoparticles During Lithiation. *ACS Nano* **2012**, *6*, 1522–1531.
21. Su, Q. M.; Dong, Z. M.; Zhang, J.; Du, G. H.; Xu, B. S. Visualizing the Electrochemical Reaction of ZnO Nanoparticles with Lithium by *in Situ* TEM: Two Reaction Modes Are Revealed. *Nanotechnology* **2013**, *24*, 255705.
22. Schmid, H. K.; Mader, W. Oxidation States of Mn and Fe in Various Compound Oxide Systems. *Micron* **2006**, *37*, 426–432.
23. Taftø, J.; Krivanek, O. L. Site-Specific Valence Determination by Electron Energy-Loss Spectroscopy. *Phys. Rev. Lett.* **1982**, *48*, 560–563.
24. Zhang, J. J.; Sun, Y. F.; Yao, Y.; Huang, T.; Yu, A. S. Lysine-Assisted Hydrothermal Synthesis of Hierarchically Porous Fe_2O_3 Microspheres as Anode Materials for Lithium-Ion Batteries. *J. Power Sources* **2013**, *222*, 59–65.
25. Zhang, J. J.; Huang, T.; Liu, Z. L.; Yu, A. S. Mesoporous Fe_2O_3 Nanoparticles as High Performance Anode Materials for Lithium-Ion Batteries. *Electrochem. Commun.* **2013**, *29*, 17–20.
26. Xiao, H.; Xia, Y.; Zhang, W. K.; Huang, H.; Gan, Y. P.; Tao, X. Y. Template-Free Synthesis of Hollow a-Fe_2O_3 Microcubes for Advanced Lithium-Ion Batteries. *J. Mater. Chem. A* **2013**, *1*, 2307–2312.
27. Zhu, J. X.; Yin, Z. Y.; Yang, D.; Sun, T.; Yu, H.; Hoster, H. E.; Hng, H. H.; Zhang, H.; Yan, Q. Y. Hierarchical Hollow Spheres Composed of Ultrathin Fe_2O_3 Nanosheets for Lithium Storage and Photocatalytic Water Oxidation. *Energy Environ. Sci.* **2013**, *6*, 987–993.
28. Larcher, D.; Masquelier, C.; Bonnin, D.; Chabre, Y.; Masson, V.; Leriche, J. B.; Tarascon, J. M. Effect of Particle Size on Lithium Intercalation into a-Fe_2O_3. *J. Electrochem. Soc.* **2003**, *150*, A133–A139.
29. Chang, K.; Chen, W. X.; Honma, I. Enhanced Cyclic Performance and Lithium Storage Capacity of SnO_2/Graphene Nanoporous Electrodes with Three-Dimensionally Delaminated Flexible Structure. *Nano Lett.* **2009**, *9*, 72–75.